Advances in Nano Research, *Vol. 12, No. 3 (2022) 291-300*
https://doi.org/10.12989/anr.2022.12.3.291

Hydrogen-bonded clusters in transformed Lewis acid to new Brønsted acid over WO_x/SiO_2 catalyst

Sirawat Boonpai[1c], Sippakorn Wannakao[2c], Joongjai Panpranot[1a], Supareak Praserthdam[1b], Prae Chirawatkul[3c] and Piyasan Praserthdam[*1]

[1]*Center of Excellence on Catalysis and Catalytic Reaction Engineering, Department of Chemical Engineering, Faculty of Engineering, Chulalongkorn University, Bangkok 10330, Thailand*
[2]*SCG Chemicals, Co., Ltd., 1 Siam-cement Rd, Bang sue, Bangkok 10800, Thailand*
[3]*Synchrotron Light Research Institute (Public Organization) 111 University Avenue, Muang District, Nakhon Ratchasima 30000, Thailand*

(*Received August 30, 2020, Revised January 8, 2021, Accepted January 9, 2021*)

Abstract. The behavior of hydrogen species on the surface of the catalyst during the Lewis acid transformation to form Brønsted acid sites over the spherical silica-supported WO_x catalyst was investigated. To understand the structure-activity relationship of Lewis acid transformation and hydrogen bonding interactions, we explore the potential of using the in situ diffuse reflection infrared Fourier transform spectroscopy (DRIFTS) with adsorbed ammonia and hydrogen exposure. From the results of in situ DRIFTS measurements, Lewis acid sites on surface catalysts were transformed into new Brønsted acid sites upon hydrogen exposure. The adsorbed NH_3 on Lewis acid sites migrated to Brønsted acid sites forming $NH4^+$. The results show that the dissociated H atoms present on the catalyst surface formed new Si−OH hydroxyl species − the new Brønsted acid site. Besides, the isolated Si−O−W species is the key towards H-bond and Si−OH formation. Additionally, the H atoms adsorbed surrounding the Si−O−W species of mono-oxo $O=WO_4$ and di-oxo $(O=)_2WO_2$ species, where the Si−O−W species are the main species presented on the Inc-SSP catalysts than that of the IWI-SSP catalysts.
Keywords: acid transformation; Brønsted acid; *in situ* DRIFTS; Lewis acid; silica; tungsten oxide

1. Introduction

The designing and studying of silica-supported tungsten oxide catalysts (SiO_2-WO_x) have received significant attention and become a popular topic since it presents both Lewis and Brønsted acidic sites, which encourages interesting properties for a wide range of applications (e.g., photocatalytic efficiency, selective oxidations, petro-chemical industry, etc.) (Quan *et al*. 2020, Kiani *et al*. 2020, Watmanee *et al*. 2019, Kiani *et al*. 2019, Maity *et al*. 201, Mirtaheri *et al*. 20168). The acidic active sites on its surface materials are commonly considered one of the most versatile applications (Saelee *et al*. 2021, Zhou *et al*. 2014, Zhang *et al*. 2013). Additionally, Song *et al*. (2015) described that the oxygen-deficient surface of WO_x can certainly activate molecular hydrogen in both kinetics and thermodynamics. Its oxygen vacancies site can serve as shallow donors, enhancing capability for hydrogen dissociation (Huang *et al*. 2015). Therefore, the study of hydrogen surface behavior and acidic property on WO_x catalysts has recently attracted a great degree of academic interest. The perception of these properties can provide valuable information for understanding their catalytic properties and surface chemistry.

The transformation of Lewis acid is an interesting issue that Lewis acid sites can be converted to new Brønsted acid sites during catalytic reactions (Ebitani *et al*. 1991, Ebitani *et al*. 1992). This phenomenon involves the catalytic process under hydrogen dissociation to become the hydrogen spillover and electron transfer process on solid acid catalysts. The O atoms around Lewis acid sites can be stabilized with a released electron from H atoms, then they lose their function and exhibit a strong Lewis basicity described by Hattori and Shishido (1997). Ueda *et al*. (2000) reported that hydrogen spillover should enhance the change of Lewis acid site by desorption of adsorbed pyridine on SiO_2-supported noble metal (Pd, Pt, Rh, and Ir). Also, Guntida *et al*. (2018) suggested that the transformation of Lewis acid was presented over the physically mixing of Pt/Al_2O_3 and oxide materials (e.g., SiO_2 and Al_2O_3) by the hydrogen dissociation process on Pt particles. Recently, the enhancement of tungstate W^{5+} species and its oxygen vacancy were found to play an important role in activating the acid site's transformation (Boonpai *et al*. 2020, Guntida *et al*. 2020).

Silica supports of the WO_x catalyst have commonly been used in catalytic systems, in which the nature of support can improve the surface tungsten species. The silica-supported WO_x catalysts presented a different structure-activity relationship over their surface (Hu *et al*. 2011, Liu *et al*. 2012). While the impregnation of tungsten species onto silica exhibits low dispersion due to the formation of polytungstate and crystalline WO_3, the incorporation of tungsten species to silica can provide a

*Corresponding author, Professor,
E-mail: piyasan.p@chula.ac.th
[a] Professor, E-mail: joongjai.p@chula.ac.th
[b] Assistant Professor, E-mail: supareak.p@chula.ac.th
[c] Ph.D., E-mail: prae@slri.or.th

ISSN: 2287-237X (Print), 2287-2388 (Online)

high dispersion by embedding of W species to silica framework described by Hu *et al*. (2006). Although the transformation of Lewis acid was studied as the previous literature mentioned above, the influence of Lewis acid transformation to Brønsted acid between H-bonding interaction and W species on the silica support is ambiguous. Therefore, this issue is necessary to be further studied to better comprehend the surface tungstate species on mesoporous silica for the transformation of Lewis acid, which could be beneficial information for designing the solid acid catalyst in the future.

Herein the influence of Lewis acid transformation to Brønsted acid between H-bonding interaction and W species on the silica support was investigated over silica-supported WO_x catalysts. The mesoporous spherical silica nanoparticle (SSP) was used as silica support due to its advantageous properties and diverse functionalization (Zeng *et al*. 2021, Lv *et al*. 2016, Watmanee *et al*. 2018). To explore the structure-activity relationship of Lewis acid transformation, the sample was synthesized via two techniques: (i) incorporation of tungsten oxide with the sol-gel method (Inc-SSP) and (ii) incipient wetness impregnation method (IWI-SSP) to SSP support. The powerful method of *in situ* diffuse reflection infrared Fourier transform spectroscopy (DRIFTS) with adsorbed ammonia and hydrogen exposure was used to study the surface molecular on the surface catalyst (Guntida *et al*. 2018, Yfanti and Lemonidou 2018, Boonpai *et al*. 2020). However, the results could provide the benefits information about the insight into the nature of acid site transformation on solid acid catalysts under hydrogen conditions such as hydrogenation, dehydrogenation, organic transformations, and polymerization (Shen *et al*. 2017, Zhang *et al*. 2014, Xie and Wan 2019, 2020, 2021).

2. Results and discussion

2.1 Characterizations of catalysts

The prepared sample is well uniformly dispersed during the synthesis, evidenced by Energy-dispersive X-ray spectroscopy (EDS) as shown in Table 1. The content of W surface concentration shows a similar W content in Inc-SSP (0.95 at%) and IWI-SSP (0.93 at%) catalysts. Besides, the BET results show that pore size, pore volume, and surface area are not significantly changed. This indicates that the preparation methods (i.e., impregnation and incorporation) are not significantly cause the morphology of catalysts. TEM and SEM images in Fig. 1 show the spherical shape of SSP materials, in which the IWI-SSP presents more crystalline WO_3 than Inc-SSP over their surface. This result is well agreeable with XRD and Raman analysis, as shown in Fig. 3. The IWI-SSP catalyst presents the highest intensity peaks of monoclinic WO_3 patterns on XRD (Bera and Koner 2012, Ansari *et al*. 2019). Also, the Raman spectra of IWI-SSP show a higher intensity of stretching mode of W−O−W at 808 cm^{-1} than Inc-SSP catalyst (Horsley *et al*. 1987, Ross-Medgaarden and Wachs 2007). The results are agreeable with the Wachs group that the crystalline WO_3 nanoparticles will be presented on WO_x/

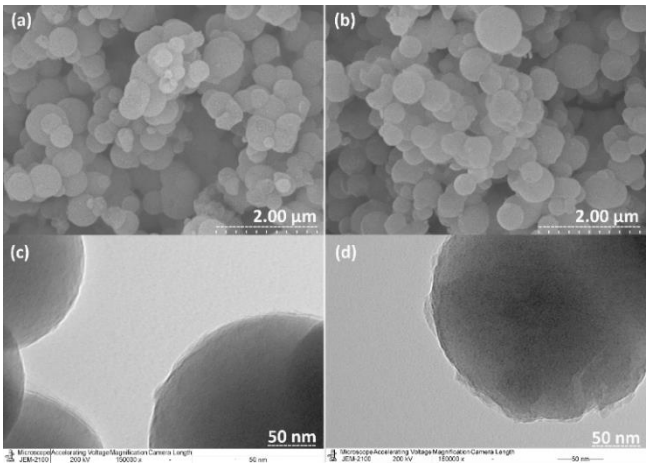

Fig. 1 SEM images of (a) Inc-SSP, (b) IWI-SSP, and TEM images of (c) Inc-SSP, (d) IWI-SSP

Table 1 Porous texture and element surface concentration of SSP-supported WO_x catalysts

Sample	Porous texture			SEM-EDS elemental analysis		
	S_{BET}[a] (m^2/g)	V[b] (cm^3/g)	P[c] (nm)	W (at%)	O (at%)	Si (at%)
Inc-SSP	892	0.68	3.1	0.95	62.68	36.37
IWI-SSP	944	0.55	2.3	0.93	58.20	40.87

[a] Specific surface area
[b] Total pore volume (P/P_0 = 0.990)
[c] Average pore size

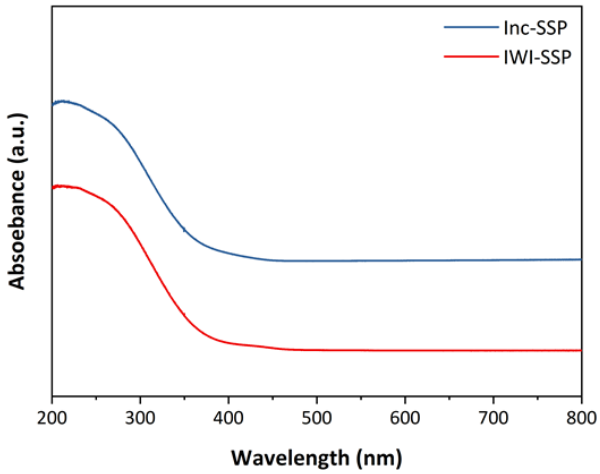

Fig. 2 UV-vis spectra of SSP-supported WO_x catalysts

SiO_2 at W loading ≥8 wt% (Lwin *et al*. 2016). However, the isolated tetrahedral ($[WO_4]^{2-}$) and octahedral polytungstate ($[WO_6]^{n-}$) species are also detected by UV-vis DRS (see Fig. 2), which is shown in at the band 225 and 262 nm (Bhuiyan *et al*. 2013, Wu *et al*. 2016), respectively.

The tungsten oxide structure was studied by X-ray absorption near-edge structure (XANES) spectroscopy, which provided the W L1 edge XANES spectra and Fitting pre-edge peaks. The observed XANES pre-edge peaks in Fig. 4(a) indicate the pre-edge feature of WO_4 coordinated structures and isolated tungstate oxo species (mono-oxo $O{=}WO_4$ and di-oxo $(O{=})_2WO_2$), which absorbing W atom is

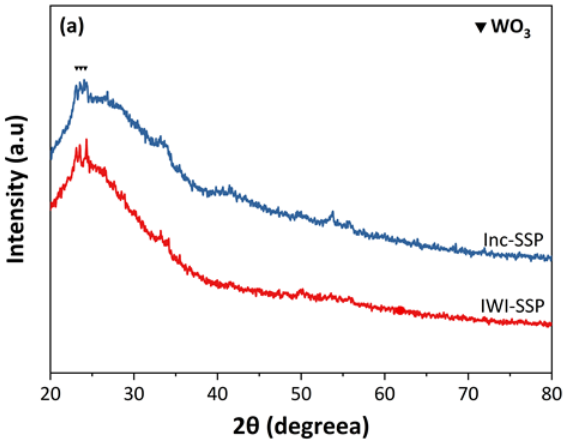

(a) XRD patterns

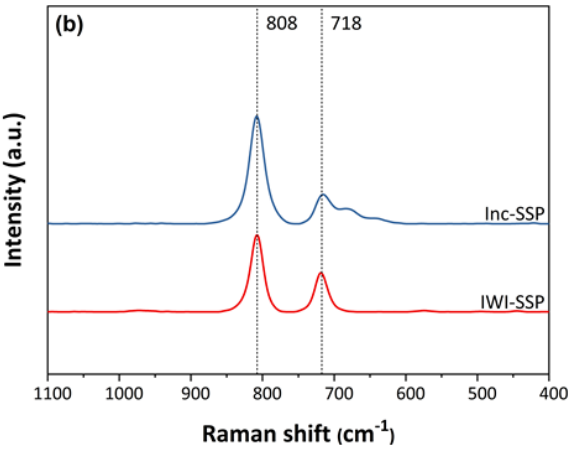

(b) Raman spectra

Fig. 3 XRD patterns and Raman spectra of catalysts

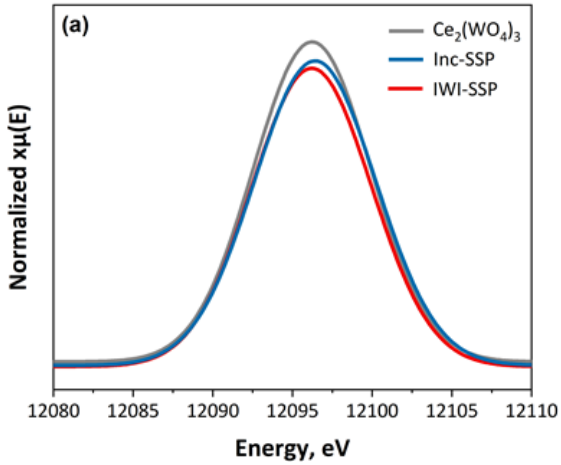

(a) Normalized XANES spectra

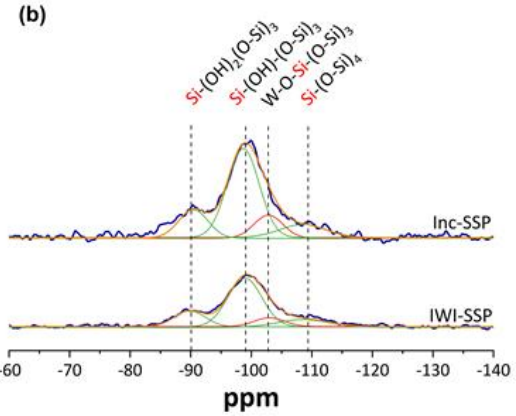

(b) ^{29}Si NMR

Fig. 4 Normalized XANES spectra collected at the W L1 edge and ^{29}Si NMR of catalysts

displaced from the inversion symmetry center (Howell *et al*. 2016, Lwin *et al*. 2016, Watmanee *et al*. 2019). The results reveal that IWI-SSP and Inc-SSP catalysts present both dioxo and mono-oxo species as similar pre-edge features characteristic of standard compound $Ce_2(WO4)_3$, which contains only isolated WO_4 sites (Lwin *et al*. 2016, Wu *et al*. 2018). However, the Inc-SSP catalyst exhibit a higher intensity of pre-edge peaks than the IWI-SSP catalyst, indicating that the isolated tungstate oxo species is mostly presented on the surface of the Inc-SSP catalyst. The Si−O−W species is contained in the tungsten oxide structure types of mono-oxo $O{=}WO_4$ and di-oxo $(O{=})_2WO_2$ species, in which W atoms flanked by either two or four −O−Si moieties) (Wu *et al*. 2018, Watmanee *et al*. 2019).

Additionally, the formed Si−O−W species are further evidenced by the ^{29}Si MAS NMR in Fig. 4(b), and its fitting results are shown in Table 2. There are four peaks at the chemical shift −91.3, −99.2, −103.7, and −108.1 ppm, assigned to different species of $Si{-}(OH)_2(O{-}Si)_2$, $Si{-}(OH)(O{-}Si)_3$, $W{-}O{-}Si{-}(O{-}Si)_3$, and $-Si{-}(O{-}Si)_4$, respectively (Klepel *et al*. 2004, Hu *et al*. 2007b, Wu *et al*. 2018). According to Table 2, the $W{-}O{-}Si{-}(O{-}Si)_3$ structure more occurs over Inc-SSP than IWI-SSP catalyst as agreed with W L1 edge XANES results. Klepel *et al*. (2004) suggested that this structure indicated the silicon is flanked by one W atom and three Si atoms in W-incorporated silicate catalysts.

Table 2 Deconvoluted results of relative peaks ^{29}Si NMR analysis of catalysts

Sample	Deconvoluted results of ^{29}Si NMR (%)			
	$Si{-}(OH)_2$ $(O{-}Si)_2$	$Si{-}(OH)$ $(O{-}Si)_3$	$W{-}O{-}Si{-}$ $(O{-}Si)_3$	$Si{-}$ $(O{-}Si)_4$
Inc-SSP	16.9	57.5	13.4	12.2
IWI-SSP	17.2	58.2	10.5	14.1

Thus, the three species of $Si{-}(O{-}Si)_4$, $Si{-}(OH)(O{-}Si)_3$, and $Si{-}(OH)_2(O{-}Si)_2$ are commuted to $W{-}O{-}Si{-}(O{-}Si)_3$ by the combining of W species and −OH groups (Hu *et al*. 2007a, b). The results indicate that W species on Inc-SSP can be mostly embedded into their bulk silica support to generate Si−O−W species instead of aggregating together to form the crystalline phase, which well agrees with TEM, Raman, W L1 edge XANES, and ^{29}Si MAS NMR results.

2.2 Transformation of Lewis to Brønsted acid on surface catalysts

The transformation of Lewis acid was studied by *in situ* DRIFTS of adsorbed ammonia with hydrogen exposure, as shown in Fig. 5. All samples show IR spectra of the surface acidity of Lewis acid sites at the band 1280 cm^{-1} and 1622

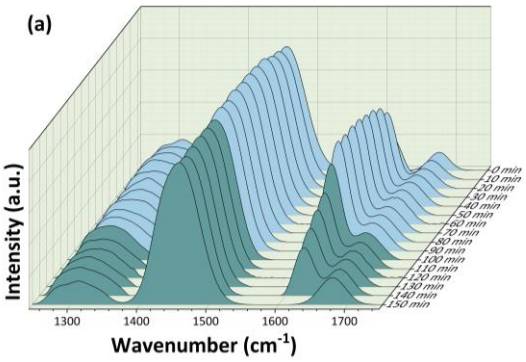

(a) XRD patterns

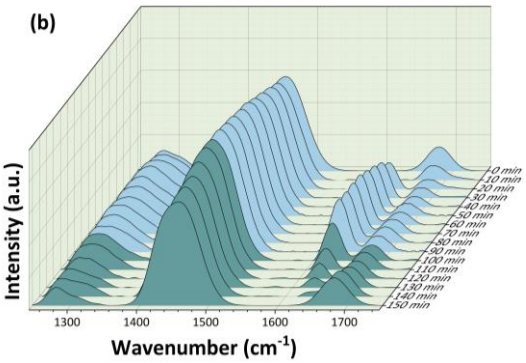

(b) Raman spectra

Fig. 5 *In situ* DRIFTS spectra adsorbed NH3 upon hydrogen exposure for 0-90 min (blue region) and nitrogen purging for 100-150 min (green region) of catalysts

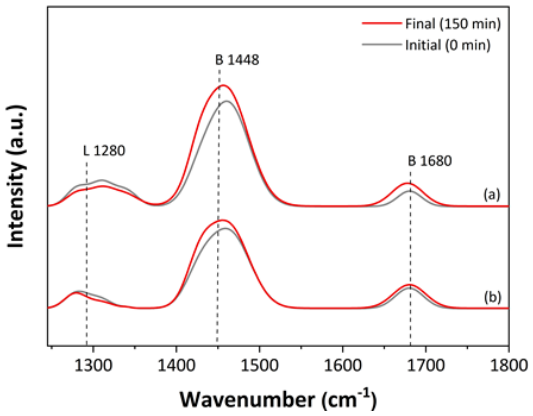

Fig. 6 *In situ* DRIFTS spectra of adsorbed NH3 upon hydrogen exposure at initial (red line) and final (grey line) over catalysts; Inc-SSP (a), and IWI-SSP (b)

cm^{-1} (adsorbed NH_3), and Brønsted acid sites at the bands 1448 and 1680 cm^{-1} (adsorbed NH_4^+) (Wu *et al*. 2012, Vorakitkanvasin *et al*. 2017, Xu *et al*. 2017). The sample was adsorbed by ammonia to detect the initial Lewis and Brønsted acid sites. After that, the sample was exposed to hydrogen for 90 min (blue peaks of 0-90 min) to investigate the Lewis acid transformation to Bronsted acid during the hydrogen exposure. Finally, the sample was switched to nitrogen for 60 min (green peaks of 90-150 min) to relieve the possible effect of moisture at around 1410, 1609, and 1700 cm^{-1} (Daniel *et al*. 1987, Persson *et al*. 1992). To

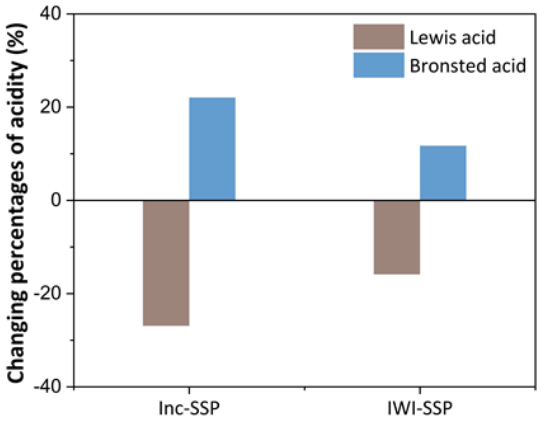

Fig. 7 Decreasing percentages of Lewis acid sites (brown) and Increasing percentages of Brønsted acid sites (blue) over catalysts

observe the change of acid sites, the IR spectra at the initial stage (0 min) and the final stage (150 min) were compared in Fig. 6. The results show that the Brønsted acid sites were generated at around 1448 and 1680 cm^{-1}, while Lewis acid sites at 1280 cm^{-1} were relatively decreased. Thus, Lewis acid sites on surface catalysts were transformed into new Brønsted acid sites upon hydrogen exposure. Besides, our results are well agreeable with previous literature (Guntida *et al*. 2018, 2020). The reduced WO_x catalyst can provide the lower oxidation state and its oxygen vacancy sites, in which they can certainly generate H atoms and hydrogen spillover under the hydrogen dissociation process (Song *et al*. 2015, Boonpai *et al*. 2020). The H atoms can release an electron and stabilize at around O atoms of Lewis acid sites, leading to its acid site transformation (Hattori and Shishido 1997). The weak interaction between WO_x and SiO_2 allowed hydrogen accessibility led to a high amount of Lewis acid transformation (Guntida *et al*. 2020). In our results, the changing percentages of this acidity are shown in Fig. 7 by the consideration of equations in the experimental section. It is clearly shown that the performance of Lewis acid transformation on Inc-SSP is better than the IWI-SSP catalyst. Therefore, the Inc-SSP catalyst exhibited mostly W species that promote the hydrogen-bonded clusters and the transformation of its acid sites. However, the IWI-SSP catalyst has a low amount of Lewis acid sites of 1622 cm^{-1} at the initial (0-10 min). Since the IWI-SSP catalyst was prepared by the incipient wetness impregnation method between tungsten oxide and silica, it is generally found that the WO_3/SiO_2 catalysts have low Lewis acid intensity due to the W species that presented on the surface catalyst (Gayapan *et al*. 2018).

2.3 Hydrogen-bonded clusters on surface catalyst

To understand the structure-activity relationship of hydrogen bonding interactions, the *in situ* DRIFTS with the only hydrogen exposure was applied to investigate the hydrogen surface behavior on catalysts (see Fig. 8). As shown in Figs. 8(a) and 8(b), the intensities of all spectra were increased during hydrogen exposure, indicating the hydrogen-bonding on their surface catalysts. The major

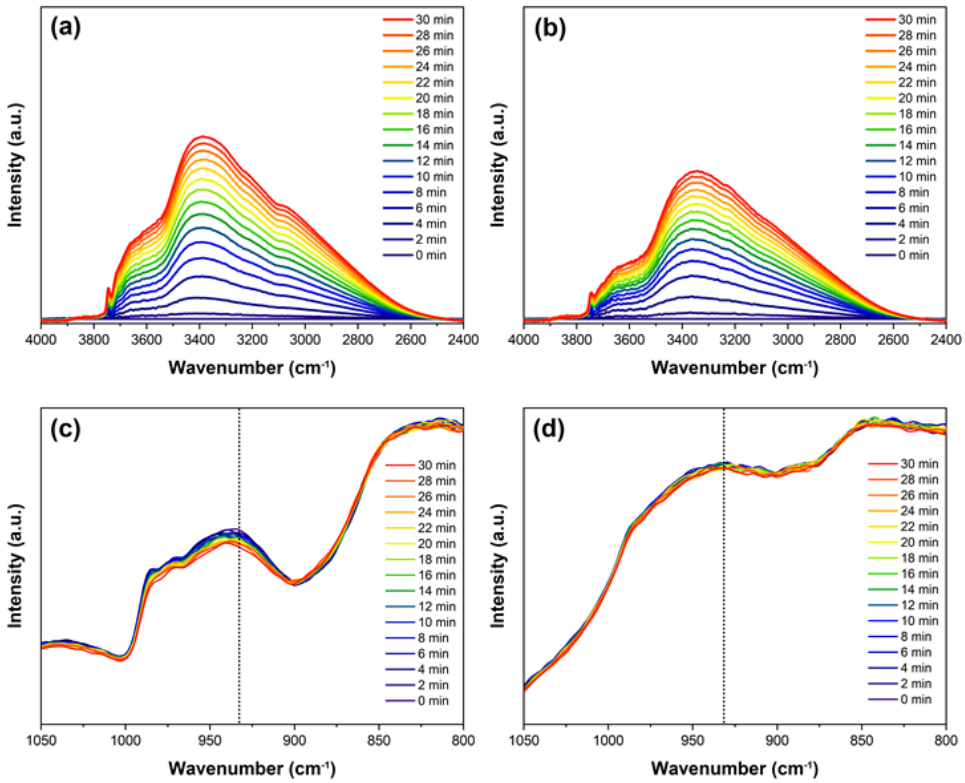

Fig. 8 *In situ* DRIFTS spectra with hydrogen exposure of catalysts; Inc-SSP (a,c), and IWI-SSP (b,d)

band at 3455 and 3646 cm^{-1} are related to the isolated silanol Si−OH groups on the surface, which provides opportunities to form hydrogen bonds (Wallin *et al*. 2005, Aziz *et al*. 2017). Besides, the sharp band was increased at 3741 cm^{-1} assigned to surface silanols Si−OH vibration (Chirkin *et al*. 2012, Bendjeriou-Sedjerari *et al*. 2016). The results reveal that the hydroxyl (−OH) groups were generated on the surface catalyst during hydrogen exposure. The band intensity of the formed Si−OH species (i.e., 3455, 3646, and 3741 cm^{-1}) is relatively increased with Inc-SSP > IWI-SSP. Thus, the result implies that the OH groups prefer to generate over silica surface of Inc-SSP catalysts than the IWI-SSP catalysts. Additionally, the major band at 921-970 cm^{-1} in Fig. 8(c) and 6d of the Inc-SSP catalysts were decreased during the hydrogen exposure, which was assigned to Si−O−W species (Yang *et al*. 2005, Hu *et al*. 2007a, Watmanee *et al*. 2019). Meanwhile, the Si−O−W species seemed a little decreasing in the IWI-SSP catalyst. The results indicate that the Si−O−W species could be consumed, while the Si−OH species were simultaneously generated during the process. Thus, the Si−O−W species should play a key role in the H atoms to form Si−OH formation. Shen *et al*. (2017) reported that the molecular hydrogen was hydrogenated on Ru/SBA-15 catalysts to form H atoms, in which the H species were adsorbed on the residing along with Ru-SiO_2 interface. Also, the surface coverage of new hydroxyl (OH) groups were formed at the vicinity of the Pt particles under the hydrogen atmosphere, in which the interface of Pt-silica is a major importance for the OH group formation (Wallin *et al*. 2005). In this process, the electron-transfer process of dissociated H species also occurred at the Pt-SiO_2 interface (Wallin *et al*. 2005). Moreover, Qian *et al*. also suggested the process of CH_4 reforming with CO_2 over Rh/MCF catalysts, in which the spillover hydrogen atoms from CH_4 decomposition on rhodium surface were found to adsorb on Si−O−Si bridged oxygen sites of MCF and to form surface Si−OH groups (Qian *et al*. 2015). Therefore, the results of Si−OH formation can indicate the activation/dissociation of molecular hydrogen to form the adsorbed atomic hydrogen on the silica surface. In our results, the Si−OH species were increased and Si−O−W species were decreased during hydrogen exposure, indicating that H atoms should be adsorbed at Si−O−W species to form the new Si−OH species surrounding its sites.

2.4 Influence of Lewis acid transformation to Brønsted acid between H-bonding interaction and W species

The results are further studied by H_2-TPD analysis in Fig. 9. The samples show two hydrogen desorption peaks. The first peaks (I) at temperatures range < 200°C were attributed to hydrogen desorption on the metal site, while the second peaks (II) at temperatures ranging 200-400°C were related to spillover hydrogen onto the silica support (Zhang *et al*. 2014). Song *et al*. reported that the oxygen-deficient surface of tungsten oxide can activate hydrogen very easily in kinetics and thermodynamics (Song *et al*. 2015). The H atoms were generated and migrated to the silica support, as seen in peaks II of Fig. 9. The Inc-SSP catalyst shows a higher intensity peak (II) than the IWI-SSP

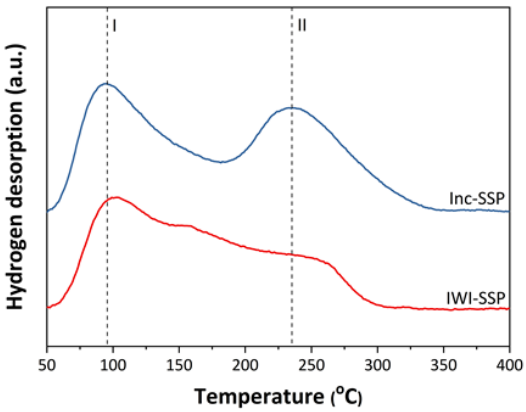

Fig. 9 Hydrogen temperature-programmed desorption profiles of catalysts

Fig. 10 Schematic model of hydrogen-bonded clusters in Lewis acid transformation to new Brønsted acid over catalysts

catalyst. This result indicates the high accessibility of hydrogen spillover over the Inc-SSP catalyst. The molecular hydrogen was dissociated to form spillover hydrogen onto the silica support. The final state of spillover hydrogen is involved in the hydroxyls −OH groups formation, in which the oxygen sites can accept the H atoms or ions (Rozanov and Krylov 1997). Generally, the formed new hydroxyl groups should provide the Brønsted acid sites (Hara *et al*. 2015, Yun *et al*. 2016). However, our results show that the increase of new Si−OH formation is related to the Lewis acid transformation, in which the Inc-SSP catalyst shows a higher performance than those of the IWI-SSP catalyst. flanked by either two/four −O−Si moieties) (Wu *et al*. 2018, Watmanee *et al*. 2019). The isolated di-oxo and mono-oxo types are presented on WO_x/SiO_2 catalyst as reported by Wachs group (Lwin *et al*. 2016). Recently, Subramaniam group reported that the W−O−Si species in di-oxo and mono-oxo species are active site precursors for olefins metathesis with W-Incorporated Silicates (Wu *et al*. 2018). These are agreed with our results that the Si−O−W species, in which the existence of isolated tungstate oxo species was supported by the W L1 edge XANES technique, is a key role in the formation of new Si−OH species subsequent to the Lewis acid transformation to new Brønsted acid sites as confirmed by the results of *in situ* DRIFTS.

The schematic model of the effect of hydrogen surface behavior on the Lewis acid transformation to Brønsted acid over catalysts is shown in Fig. 10. Molecular hydrogen is dissociated on WO_x sites to form hydrogen spillover. Firstly, H atoms can migrate to adsorb surrounding the oxygen sites of Si−O−W species, leading to the formation of new Si-OH groups. Therefore, the *in situ* DRIFTS with hydrogen exposure experiments detected the increase of Si-OH groups. However, these formed hydroxyl groups should provide a new Brønsted acid site. Secondly, H atoms can migrate to adsorb at Lewis acid sites, leading to the transformation of Lewis acid. The H atoms can release an electron to Lewis acid sites. Then it can lose its property and can desorb its NH_3. However, this NH_3 should be migrated to adsorb at new Brønsted acid sites or new hydroxyl groups, and then the Brønsted acid sites donate the protons to form NH_4^+. Thus, the *in situ* DRIFTS with adsorbed ammonia experiments detected the increase of NH_4^+. Additionally, the possible mechanism is proposed as follows Eqs. (1)-(5):

$$2NH_{3(g)} \leftrightarrow 2NH_{3(a)} \quad (1)$$

$$H_2 \leftrightarrow 2H \quad (2)$$

$$2H \leftrightarrow 2H^+ + 2e \quad (3)$$

$$2H^+ + 2 \bullet (Si-O-W) \leftrightarrow 2H \bullet (Si-O-W) \quad (4)$$

$$2NH_{3(a)} + 2H \bullet (Si-O-W) \leftrightarrow 2NH_4 \bullet (Si-O-W) \quad (5)$$

However, the formed OH groups on the catalyst surface are usually active precursors for adsorbed substances (Hair 1975, Inaki *et al*. 2002, van Grieken *et al*. 2007, Yue *et al*. 2008, Azmi *et al*. 2020). Therefore, our results can provide the valuable information that the Si−OH species and Brønsted acid, which can be formed under the hydrogen atmosphere, can affect the pathway of the reaction with hydrogen. Additionally, the Si−OH species could be generated over Rh/MCF under CH_4 dry reforming reaction (Qian *et al*. 2015). The CH_4 was decomposed into CH_3* and H*, then H atoms adsorbed on bridged oxygen sites (Si−O−Si) of the support to form Si−OH groups, which can improve the rate of dry reforming reaction (Qian *et al*. 2015). Fujimoto *et al*. (1993) also reported that the hydrogen spillover could participate as a Brønsted acid site on the zeolite, leading to hydrogenation. Therefore, this work can provide the beneficial information for the influence of W species on hydrogen bonding interactions presented on the catalyst surface, which enhances the surface designs further catalytic performance.

3. Experimental

3.1 Material synthesis

Spherical silica nanoparticle (SSP) was used as support for catalysts. The SSP was synthesized using the sol-gel

method with tetraethoxysilane (TEOS) for the silica source and cetyl trimethyl ammonium bromide (CTAB) for the structure-directing agent. The solution contains H_2O, C_2H_5OH, NH_3, TEOS, and CTAB with the composition ratio as reported by literatures (Watmanee *et al*. 2018). Firstly, C_2H_5OH, H_2O, and NH_3 were mixed, and then CTAB was added to this solution with a stirring rate of 350 rpm for 15 min. Then, the TEOS was slowly dropped to this obtained solution with a stirring rate of 350 rpm for 120 min. Secondly, the solution was then stirred for 120 min to become the gel, and then it was filtrated and diluted with H_2O to get a *pH* of 7. After that, the filtrated sample was kept overnight in an oven at 110°C. Finally, the dried sample was heated to 550°C with 2°C/min for 6 h under the calcination in the air to obtain the SSP support. For the impregnated catalysts (IWI-SSP), the SSP support was impregnated by the tungsten precursor solution of ammonium metatungstate hydrate ($(NH_4)_6H_2W_{12}O_{40}\cdot xH_2O$) using incipient wetness impregnation method, and then the sample was dried under ambient for 2 h. After that, the filtrated sample was kept overnight in an oven at 110°C. Finally, the dried sample was heated to 550°C with 10°C/min for 8 h under the calcination in air. The 8%wt of W content by weight was denoted IWI-SSP. For the incorporated catalysts (Inc-SSP), the preparation of SSP support with the sol-gel method was modified by adding the tungsten precursor and TEOS to the solution simultaneously. The 8%wt of W content by weight was denoted as Inc-SSP.

3.2 In situ DRIFTS with hydrogen exposure experiments

The vibrational of hydrogen interactions presented on the catalyst surface was investigated by the *in situ* diffuse reflectance infrared Fourier transform spectroscopy (DRIFTS) with hydrogen exposure using Bruker's Vertex-70 FT-IR research spectrometer. The Praying Mantis™ accessory was used for the diffuse reflectance reaction chamber to study catalysts and reactions in controlled environments. The sample was carried out into KBr windows. Firstly, the sample was pre-treated using H_2 and N_2 gas flow 10 ml/min at 500°C for 1 h, and then it was heated to 550°C for 30 min and cooling down to 100°C under an N_2. To study the transformation of the acid site, the sample was adsorbed by ammonia (15% NH_3/He) flow 10 ml/min, and then the sample was exposed to H_2 and N_2 at 100°C under atmospheric pressure. To study hydrogen-bonded clusters, the sample was exposed to H_2 at 100°C under atmospheric pressure. The IR spectra were automatically recorded using an MCT detector. The IR spectra were subtracted with their first spectra at 0 min. The decreased percentage of Lewis acid sites was considered using the IR band of 1280 cm^{-1} and the calculation of Eq. (6), while the increasing percentage of Bronsted acid sites was considered using the IR band of 1448 and 1680 cm^{-1} and the calculation of Eq. (7).

$$\text{Decreasing of Lewis acid sites}\,(\%) = \left(\frac{L_0 - L_i}{L_0}\right)\times 100 \qquad (6)$$

$$\text{Increasing of Bronsted acid site}\,(\%) = \left(\frac{B_0 - B_i}{B_0}\right)\times 100 \qquad (7)$$

where L_0 and B_0 refer to the deconvoluted peaks of Lewis and Bronsted acid sites at initial stage (0 min), while L_i and B_i refer to the deconvoluted peaks of Lewis and Bronsted acid sites at final stage (150 min), respectively.

3.3 Material characterizations

XRD pattern analysis was carried out using a D8 Advance of Bruker AXS using Ni-filter selecting CuK_α radiation. Brunauer-Emmett-Teller (BET) surface areas, pore volumes and pore sizes of all catalysts were performed at -196°C using a Micrometritics Chemisorbs 2750 model ASAP 2000 automated system. Transmission electron microscopy (TEM) image, and energy-dispersive X-ray spectroscopy (TEM-EDS), which were obtained on a JEOL JEM-2010 microscope equipped with a LaB6 electron gun operated at 200 kV, were used to analyze the morphology and composition of the sample. Scanning electron microscopy (SEM) experiments were investigated on a Hitachi S3400N. The UV-vis DRS was recorded using Lambda 650 spectrophotometer in the range between 200 and 500 nm. X-ray Absorption Near-Edge Structure (XANES) spectroscopy was performed in transmission mode at synchrotron light research and institute, the synchrotron Thailand central lab, which Athena and Larch software were used to analyze the data. The Fourier transform infrared spectrometer (FT-IR) was recorded with a Bruker Vertex-70 FT-IR spectrometer equipped with a Harrick Praying Mantis attachment for diffuse reflectance spectroscopy using a Mercury-Cadmium-Telluride (MCT) detector. The sample was performed in the *in situ* IR cell with KBr windows connected to the close circulating system. The sample was pretreated under mixed gas of H_2 flow (10 ml/min) and N_2 flow (10 ml/min) at 500°C for 1 h, and then it was heated to 550°C under N_2 flow for 30 min, followed by cooling to 40°C. The IR spectra were subtracted from the background spectrum obtained from the KBr sample. The solid-state ^{29}Si and ^{1}H NMR were determined by Fourier to transform nuclear magnetic resonance spectrometer 400 MHz (Solid) using a Bruker AVANCE III HD (Ascend 400 WB) spectrometer using 4 mm MAS probes at a spin rate of 8 kHz. Hydrogen temperature-programmed reduction (H_2-TPR) analysis was performed to investigate the reducibility of the sample. The measurement was carried out in a quartz microreactor by using the Micrometrics Chemisorbs 2750 automated system. The sample was pretreated in Ar (25 ml/min) at 500°C for 1 h, and then cooled down to room temperature, then it was followed by a temperature-programmed reduction by 10% H_2 in Ar (15 ml/min) from room temperature to 800°C with a heating rate of 10°C/min. Hydrogen consumption was obtained by a thermal conductivity detector (TCD). Hydrogen temperature-programmed desorption (H_2-TPD) analysis was used to investigate the adsorption behavior of hydrogen. The sample was carried out in a quartz microreactor using the Micrometrics Chemisorbs 2750 automated system. The

sample was pretreated with the mixed gas flow of H_2 (25 ml/min) and N_2 (25 ml/min) at 500°C for 1 h, and then it was heated to 550°C at a heating rate of 10°C/min under an N_2 flow for 30 min. After that, the sample was cooled to 40°C, followed by adsorption of H_2 gas flow for 30 min. Finally, the sample was purged with an N_2 flow for 1 h, and then it was heated to 400°C at a heating rate of 10°C/min under N_2 flow. The signals of hydrogen desorption were monitored by a thermal conductivity detector.

4. Conclusions

In the present work, the influence of Lewis acid transformation to Brønsted acid between H-bonding interaction and W species on the silica support was investigated over silica-supported WO_x catalysts. In the results of in situ DRIFTS, Lewis acid sites on surface catalysts were transformed to new Brønsted acid sites upon hydrogen exposure. Additionally, the Si−OH species are formed during hydrogen exposure, in which the Si−O−W species are relatively decreased. It was postulated that the isolated Si−O−W species on catalysts is a major importance for H-bonding and new Si−OH formation. The results show that the dissociated H atoms were presented and migrated onto surface catalysts to form the new hydroxyl Si−OH species, which provides a new Brønsted acid site. The H atoms can be adsorbed surrounding the Si−O−W species of mono-oxo $O=WO_4$ and di-oxo $(O=)_2WO_2$ species. The Si−O−W species are mostly presented on the Inc-SSP catalysts than the IWI-SSP catalysts. However, these results give a piece of beneficial information for the influence of W species on hydrogen bonding interactions presented on the catalyst surface, which enhances the surface designs further catalytic performance.

Acknowledgement

The authors acknowledge SCG Chemical Co., Ltd for financial support. We also acknowledge the Synchrotron Light Research Institute (Public Organization), SLRI, for the support of beamtime, and we appreciate the staff of beamline 1.1W for their assistance.

References

Ansari, S., Ansari, M.S., Satsangee, S.P. and Jain, R. (2019), "WO_3 decorated graphene nanocomposite based electro-chemical sensor: A prospect for the detection of anti-anginal drug", *Anal. Chim. Acta*, **1046**, 99-109. https://doi.org/10.1016/j.aca.2018.09.028.

Aziz, M.A.A., Puad, K., Triwahyono, S., Jalil, A.A., Khayoon, M.S., Atabani, A.E., Ramli, Z., Majid, Z.A., Prasetyokoe, D. and Hartanto, D. (2017), "Transesterification of croton megalocarpus oil to biodiesel over WO_3 supported on silica mesoporous-macroparticles catalyst", *Chem. Eng. J.*, **316**, 882-892. https://doi.org/10.1016/j.cej.2017.02.049.

Azmi, A.A., Ruhaimi, A.H. and Aziz, M.A.A. (2020), "Efficient 3-aminopropyltrimethoxysilane functionalised mesoporousceria nanoparticles for CO_2 capture", *Mater. Today Chem.*, **16**, 100273. https://doi.org/10.1016/j.mtchem.2020.100273.

Bendjeriou-Sedjerari, A., Sofack-Kreutzer, J., Minenkov, Y., Abou-Hamad, E., Hamzaoui, B., Werghi, B., Anjum, D.H., Cavallo, L., Huang K.W. and Basset, J.M. (2016), "Tungsten (VI) Carbyne/Bis(carbene) tautomerization enabled by N-Donor SBA15 surface ligands: A solid-state NMR and DFT study", *Angew. Chem. Int. Edit.*, **55**(37), 11162-11166. https://doi.org/10.1002/anie.201605934.

Bera, R. and Koner, S. (2012), "Incorporation of tungsten oxide in mesoporous silica: Catalytic epoxidation of olefins using sodium-bi-carbonate as co-catalyst", *Inorg. Chim. Acta*, **384**, 233-238. https://doi.org/10.1016/j.ica.2011.12.003.

Bhuiyan, T.I., Arudra, P., Akhtar, M.N., Aitani, A.M., Abudawoud, R.H., Al-Yami, M.A. and Al-Khattaf, S.S. (2013), "Metathesis of 2-butene to propylene over W-mesoporous molecular sieves: A comparative study between tungsten containing MCM-41 and SBA-15", *Appl. Catal. A*, **467**, 224-234. https://doi.org/10.1016/j.apcata.2013.07.034.

Boonpai, S., Wannakao, S., Panpranot, J., Jongsomjit, B. and Praserthdam, P. (2020), "Active site formation in WO_x supported on spherical silica catalysts for Lewis acid transformation to Brønsted acid activity", *J. Phys. Chem. C*, **124**(29), 15935-15943. https://doi.org/10.1021/acs.jpcc.0c03657.

Chirkin, A., Lavrenko, V., Malysheva, M. and Kuznetsova, L. (2012), "Composition and structure of functional groups on the surface of tungsten disilicide powder", *Powder Metall. Met. Ceram.*, **51**(1), 1-6. https://doi.org/10.1007/s11106-012-9388-3.

Daniel, M., Desbat, B., Lassegues, J., Gerand, B. and Figlarz, M. (1987), "Infrared and Raman study of WO_3 tungsten trioxides and WO_3, xH_2O tungsten trioxide tydrates", *J. Solid State Chem.*, **67**(2), 235-247. https://doi.org/10.1016/0022-4596(87)90359-8.

Ebitani, K., Konishi, J. and Hattori, H. (1991), "Skeletal isomerization of hydrocarbons over zirconium oxide promoted by platinum and sulfate ion", *J. Catal.*, **130**(1), 257-267. https://doi.org/10.1016/0021-9517(91)90108-G.

Ebitani, K., Tsuji, J., Hattori, H. and Kita, H. (1992), "Dynamic modification of surface acid properties with hydrogen molecule for zirconium oxide promoted by platinum and sulfate ions", *J. Catal.*, **135**(2), 609-617. https://doi.org/10.1016/0021-9517(92)90057-O.

Fujimoto, K.I., Uchijima, T., Masai, M. and Inui, T. (1993), *New Aspects of Spillover Effect in Catalysis: For Development of Highly Active Catalysts*, Elsevier, Amsterdam, Netherlands.

Gayapan, K., Sripinun, S., Panpranot, J., Praserthdam, P. and Assabumrungrat, S. (2018) "Effects of calcination and pretreatment temperatures on the catalytic activity and stability of H_2-treated WO_3/SiO_2 catalysts in metathesis of ethylene and 2-butene", *RSC Adv.*, **8**(50), 28555-28568. https://doi.org/10.1039/C8RA04949A.

Guntida, A., Suriye, K., Panpranot, J. and Praserthdam, P. (2018), "Comparative study of lewis acid transformation on non-reducible and reducible oxides under hydrogen atmosphere by in situ drifts of adsorbed NH_3", *Top. Catal.*, **61**(15), 1641-1652. https://doi.org/10.1007/s11244-018-0995-1.

Guntida, A., Suriye, K., Panpranot, J. and Praserthdam, P. (2020), "Lewis acid transformation to Bronsted acid sites over supported tungsten oxide catalysts containing different surface WO_x structures", *Catal. Today*, **358**, 354-369. https://doi.org/10.1016/j.cattod.2019.07.019.

Hair, M.L. (1975), "Hydroxyl groups on silica surface", *J. Non-Cryst. Solids*, **19**, 299-309. https://doi.org/10.1016/0022-3093(75)90095-2.

Hara, M., Nakajima, K. and Kamata, K. (2015), "Recent progress in the development of solid catalysts for biomass conversion into high value-added chemicals", *Sci. Technol. Adv. Mater.*, **16**(3), 034903. https://doi.org/10.1088/1468-6996/16/3/034903.

Hattori, H. and Shishido, T. (1997), "Molecular hydrogen-originated protonic acid site as active site on solid acid catalyst", *Catal. Surv. Asia*, **1**(2), 205-213. https://doi.org/10.1023/A:1019081031021.

Horsley, J., Wachs, I., Brown, J., Via, G. and Hardcastle, F. (1987), "Structure of surface tungsten oxide species in the tungsten trioxide/alumina supported oxide system from x-ray absorption near-edge spectroscopy and Raman spectroscopy", *J. Phys. Chem.*, **91**, 4014-4020. https://doi.org/10.1021/j100299a018.

Howell, J.G., Li, Y.P. and Bell, A.T. (2016), "Propene metathesis over supported tungsten oxide catalysts: A study of active site formation", *ACS Catal.*, **6**(11), 7728-7738. https://doi.org/10.1021/acscatal.6b01842.

Hu, J.C., Wang, Y.D., Chen, L.F., Richards, R., Yang, W.M., Liu, Z.C. abd Xu, W. (2006), "Synthesis and characterization of tungsten-substituted SBA-15: An enhanced catalyst for 1-butene metathesis", *Micropor. Mesopor. Mat.*, **93**(1-3), 158-163. https://doi.org/10.1016/j.micromeso.2006.02.019.

Hu, L., Ji, S., Jiang, Z., Song, H., Wu, P. and Liu, Q. (2007a), "Direct synthesis and structural characteristics of ordered SBA-15 mesoporous silica containing tungsten oxides and tungsten carbides", *J. Phys. Chem. C*, **111**(42), 15173-15184. https://doi.org/10.1021/jp074879h.

Hu, L., Ji, S., Xiao, T., Guo, C., Wu, P. and Nie, P. (2007b), "Preparation and characterization of tungsten carbide confined in the channels of SBA-15 mesoporous silica", *J. Phys. Chem. B*, **111**(14), 3599-3608. https://doi.org/10.1021/jp066349b.

Hu, J.Z., Kwak, J.H., Wang, Y., Hu, M.Y., Turcu, R.V. and Peden, C.H. (2011), "Characterizing surface acidic sites in mesoporous-silica-supported tungsten oxide catalysts using solid-state NMR and quantum chemistry calculations", *J. Phys. Chem. C*, **115**(47), 23354-23362. https://doi.org/10.1021/jp203813f.

Huang, Z.F., Song, J., Pan, L., Zhang, X., Wang, L. and Zou, J.J. (2015), "Tungsten oxides for photocatalysis, electrochemistry, and phototherapy", *Adv. Mater.*, **27**(36), 5309-5327. https://doi.org/10.1002/adma.201501217.

Inaki, Y., Yoshida, H., Yoshida, T. and Hattori, T. (2002), "Active sites on mesoporous and amorphous silica materials and their photocatalytic activity: An investigation by FTIR, ESR, VUV−UV and photoluminescence spectroscopies", *J. Phys. Chem. B*, **106**(35), 9098-9106. https://doi.org/10.1021/jp025768f.

Kiani, D., Sourav, S., Baltrusaitis, J. and Wachs, I.E. (2019), "Oxidative Coupling of Methane (OCM) by SiO_2-supported tungsten oxide catalysts promoted with Mn and Na", *ACS Catal.*, **9**(7), 5912-5928. https://doi.org/10.1021/acscatal.9b01585.

Kiani, D., Sourav, S., Wachs, I.E. and Baltrusaitis, J. (2020), "Synthesis and molecular structure of model silica-supported tungsten oxide catalysts for oxidative coupling of methane (OCM)", *Catal. Sci. Technol.*, **10**(10), 3334-3345. https://doi.org/10.1039/d0cy00289e.

Klepel, O., Böhlmann, W., Ivanov, E., Riede, V. and Papp, H. (2004), "Incorporation of tungsten into MCM-41 framework", *Micropor. Mesopor. Mat.*, **76**(1-3), 105-112. https://doi.org/10.1016/j.micromeso.2004.07.038.

Liu, G., Wang, X., Wang, X., Han, H. and Li, C. (2012), "Photocatalytic H_2 and O_2 evolution over tungsten oxide dispersed on silica", *J. Catal.*, **293**, 61-66. https://doi.org/10.1016/j.jcat.2012.06.003.

Lv, X., Zhang, L., Xing, F. and Lin, H. (2016), "Controlled synthesis of monodispersed mesoporous silica nanoparticles: Particle size tuning and formation mechanism investigation", *Micropor. Mesopor. Mat.*, **225**, 238-244. https://doi.org/10.1016/j.micromeso.2015.12.024.

Lwin, S., Li, Y., Frenkel, A.I. and Wachs, I.E. (2016), "Nature of WO_x sites on SiO_2 and their molecular structure–reactivity/selectivity relationships for propylene metathesis", *ACS Catal.*, **6**(5), 3061-3071. https://doi.org/10.1021/acscatal.6b00389.

Maity, N., Barman, S., Minenkov, Y., Ould-Chikh, S., Abou-Hamad, E., Ma, T., Qureshi, Z.S., Cavallo, L., D'Elia, V., Gates, B.C. and Basset, J.M. (2018), "A silica-supported monoalkylated tungsten dioxo complex catalyst for olefin metathesis", *ACS Catal.*, **8**(4), 2715-2729. https://doi.org/10.1021/acscatal.7b04304.

Mirtaheri, B., Shokouhimehr, M. and Beitollahi, A. (2016), "Synthesis of mesoporous tungsten oxide by template-assisted sol–gel method and its photocatalytic degradation activity", *J. Sol-Gel Sci. Technol.*, **82**(1), 148-156. https://doi.org/10.1007/s10971-016-4289-4.

Persson, C., Oskarsson, Å. and Andersson, C. (1992), "Tungsten (VI) complexes with bidentate coordination of the catecholate monoanion. Synthesis of $[W(O)Cl_3(O, HO{-}C_6H_4)\cdot O(C_2H_5)_2]$ and synthesis and crystal structure of $[W(O)Cl(O_2{-}C_6H_4)(O, HO{-}C_6H_4)\cdot O(C_2H_5)_2]$", *Polyhedron*, **11**(16), 2039-2044. https://doi.org/10.1016/S0277-5387(00)83159-9.

Qian, L., Cai, W., Zhang, L., Ye, L., Li, J., Tang, M., Yue, B. and He, H. (2015), "The promotion effect of hydrogen spillover on CH_4 reforming with CO_2 over Rh/MCF catalysts", *Appl. Catal., B*, **164**, 168-175. https://doi.org/10.1016/j.apcatb.2014.09.006.

Quan, H., Gao, Y. and Wang, W. (2020), "Tungsten oxide-based visible light-driven photocatalysts: Crystal and electronic structures and strategies for photocatalytic efficiency enhancement", *Inorg. Chem. Front.*, **7**(4), 817-838. https://doi.org/10.1039/c9qi01516g.

Ross-Medgaarden, E.I. and Wachs, I.E. (2007), "Structural determination of bulk and surface tungsten oxides with UV− vis diffuse reflectance spectroscopy and raman spectroscopy", *J. Phys. Chem. C*, **111**(41), 15089-15099. https://doi.org/10.1021/jp074219c.

Rozanov, V.V. and Krylov, O.V. (1997), "Hydrogen spillover in heterogeneous catalysis", *Russ. Chem. Rev.*, **66**(2), 107. https://doi.org/10.1070/RC1997v066n02ABEH000308.

Saelee, T., Limsoonthakul, P., Aphichoksiri, P., Rittiruam, M., Lerdpongsiripaisarn, M., Miyake, T., Yamashita, H., Mori, K., Kuwahara, Y., Praserthdam, S. and Praserthdam, P. (2021), "Experimental and computational study on roles of WO_x promoting strong metal support promoter interaction in Pt catalysts during glycerol hydrogenolysis", *Sci Rep*, **11**(1), 530. https://doi.org/10.1038/s41598-020-79764-3.

Shen, H., Wu, X., Jiang, D., Li, X. and Ni, J. (2017), "Identification of active sites for hydrogenation over Ru/SBA-15 using in situ Fourier-transform infrared spectroscopy", *Chin. J. Catal.*, **38**(9), 1597-1602. https://doi.org/10.1016/s1872-2067(16)62571-8.

Song, J., Huang, Z.F., Pan, L., Zou, J.J., Zhang, X. and Wang, L. (2015), "Oxygen-deficient tungsten oxide as versatile and efficient hydrogenation catalyst", *ACS Catal.*, **5**(11), 6594-6599. https://doi.org/10.1021/acscatal.5b01522.

Ueda, R., Kusakari, T., Tomishige, K. and Fujimoto, K. (2000), "Nature of spilt-over hydrogen on acid sites in zeolites: Observation of the behavior of adsorbed pyridine on zeolite catalysts by means of FTIR", *J. Catal.*, **194**(1), 14-22. https://doi.org/10.1006/jcat.2000.2906.

Van Grieken, R., Calleja, G., Serrano, D., Martos, C., Melgares, A. and Suarez, I. (2007), "The role of the hydroxyl groups on the silica surface when supporting metallocene/MAO catalysts", *Polym. React. Eng.*, **11**(1), 17-32. https://doi.org/10.1081/pre-120018583.

Vorakitkanvasin, S., Phongsawat, W., Suriye, K., Praserthdam, P. and Panpranot, J. (2017), "In situ-DRIFTS study: Influence of surface acidity of rhenium-based catalysts in the metathesis of various olefins for propylene production", *RSC Adv.*, **7**(61), 38659-38665. https://doi.org/10.1039/c7ra06181a.

Wallin, M., Grönbeck, H., Spetz, A.L., Eriksson, M. and

Skoglundh, M. (2005), "Vibrational analysis of H_2 and D_2 adsorption on Pt/SiO_2", *J. Phys. Chem. B*, **109**(19), 9581-9588. https://doi.org/10.1021/jp044759z.

Watmanee, S., Suriye, K., Praserthdam, P. and Panpranot, (2018) "Effect of surface tungstate W^{5+} species on the metathesis activity of W-doped spherical silica catalysts", *Top. Catal.*, **61**(15), 1615-1623. https://doi.org/10.1007/s11244-018-1020-4.

Watmanee, S., Suriye, K., Praserthdam, P. and Panpranot, J. (2019), "Formation of isolated tungstate sites on hierarchical structured SiO_2 and HY zeolite-supported WO_x catalysts for propene metathesis", *J. Catal.*, **376**, 150-160. https://doi.org/10.1016/j.jcat.2019.07.001.

Wu, X., Zhang, L., Weng, D., Liu, S., Si, Z. and Fan, J. (2012), "Total oxidation of propane on Pt/WO_x/Al_2O_3 catalysts by formation of metastable Ptdelta+ species interacted with WO_x clusters", *J. Hazard. Mater.*, **225**, 146-154. https://doi.org/10.1016/j.jhazmat.2012.05.011.

Wu, J.F., Ramanathan, A., Snavely, W.K., Zhu, H., Rokicki, A. and Subramaniam, B. (2016), "Enhanced metathesis of ethylene and 2-butene on tungsten incorporated ordered mesoporous silicates", *Appl. Catal. A*, **528**, 142-149. https://doi.org/10.1016/j.apcata.2016.10.004.

Wu, J.F., Ramanathan, A., Biancardi, A., Jystad, A.M., Caricato, M., Hu, Y. and Subramaniam, B. (2018), "Correlation of active site precursors and olefin metathesis activity in W-incorporated silicates", *ACS Catal.*, **8**(11), 10437-10445. https://doi.org/10.1021/acscatal.8b03263.

Xie, W., and Wan, F. (2019), "Immobilization of polyoxometalate-based sulfonated ionic liquids on UiO-66-2COOH metal-organic frameworks for biodiesel production via one-pot transesterification-esterification of acidic vegetable oils", *Chem. Eng. J.*, **365**, 40-50. https://doi.org/10.1016/j.cej.2019.02.016.

Xie, W., and Wang, H. (2020), "Immobilized polymeric sulfonated ionic liquid on core-shell structured Fe_3O_4/SiO_2 composites: A magnetically recyclable catalyst for simultaneous transesterification and esterifications of low-cost oils to biodiesel", *Renew. Energy*, **145**, 1709-1719. https://doi.org/10.1016/j.renene.2019.07.092.

Xie, W., and Wang, H. (2021), "Grafting copolymerization of dual acidic ionic liquid on core-shell structured magnetic silica: A magnetically recyclable Brönsted acid catalyst for biodiesel production by one-pot transformation of low-quality oils", *Fuel*, **283**, 118893. https://doi.org/10.1016/j.fuel.2020.118893.

Xu, H., Sun, M., Liu, S., Li, Y., Wang, J. and Chen, Y. (2017), "Effect of the calcination temperature of cerium–zirconium mixed oxides on the structure and catalytic performance of WO_3/$CeZrO_2$ monolithic catalyst for selective catalytic reduction of NO_x with NH_3", *RSC Adv.*, **7**(39), 24177-24187. https://doi.org/10.1039/c7ra03054a.

Yang, X.L., Dai, W.L., Gao, R., Chen, H., Li, H., Cao, Y. and Fan, K. (2005), "Synthesis, characterization and catalytic application of mesoporous W-MCM-48 for the selective oxidation of cyclopentene to glutaraldehyde", *J. Mol. Catal. A Chem.*, **241**(1-2), 205-214. https://doi.org/10.1016/j.molcata.2005.07.025.

Yfanti, V.L. and Lemonidou, A.A. (2018), "Mechanistic study of liquid phase glycerol hydrodeoxygenation with in-situ generated hydrogen", *J. Catal.*, **368**, 98-111. https://doi.org/10.1016/j.jcat.2018.09.036.

Yue, M.B., Sun, L.B., Cao, Y., Wang, Z.J., Wang, Y., Yu, Q. and Zhu, J.H. (2008), "Promoting the CO_2 adsorption in the amine-containing SBA-15 by hydroxyl group", *Micropor. Mesopor. Mat.*, **114**(1-3), 74-81. https://doi.org/10.1016/j.micromeso.2007.12.016.

Yun, D., Yun, Y.S., Kim, T.Y., Park, H., Lee, J.M., Han, J.W. and Yi, J. (2016), "Mechanistic study of glycerol dehydration on Brønsted acidic amorphous aluminosilicate", *J. Catal.*, **341**, 33-43. https://doi.org/10.1016/j.jcat.2016.06.010.

Zeng, Y., Zhu, X., Xie, J., and Chen, L. (2021), "Ionic liquid coated magnetic core/shell $CoFe_2O_4$@SiO_2 nanoparticles for the separation/analysis of trace gold in water sample", *Adv. Nano Res.*, **10**(3), 295-312. https://doi: 10.12989/anr.2021.10.3.295.

Zhang, X., Hu, C., Bai, H., Yan, Y., Li, J., Yang, H., Lu, X. and Xi, G. (2013), "Construction of self-supported three-dimensional TiO_2 sheeted networks with enhanced photocatalytic activity", *Sci. Rep.*, **3**(1), 3563. https://doi.org/10.1038/srep03563.

Zhang, Y., Zhou, Y., Shi, J., Zhou, S., Sheng, X., Zhang, Z. and Xiang, S. (2014), "Comparative study of bimetallic Pt-Sn catalysts supported on different supports for propane dehydrogenation", *J. Mol. Catal. A Chem.*, **381**, 138-147. https://doi.org/10.1016/j.molcata.2013.10.007.

Zhou, Z., Kong, B., Yu, C., Shi, X., Wang, M., Liu, W., Sun, Y., Zhang, Y., Yang, H. and Yang, S. (2014), "Tungsten oxide nanorods: An efficient nanoplatform for tumor CT imaging and photothermal therapy", *Sci. Rep.*, **4**(1), 3653. https://doi.org/10.1038/srep03653.

JL